Transport in-between Edge Localized Modes in the Pedestal of ASDEX Upgrade

B. Kurzan, E. Wolfrum, A. Burckhart, T. Pütterich, B. Wieland, R. Fischer, P. Schneider, W. Suttrop, H. Zohm, ASDEX Upgrade Team

Max-Planck-Institut für Plasmaphysik, EURATOM Association, Garching, Germany

E-mail contact of main author: Bernd.Kurzan@ipp.mpg.de

Abstract. The good confinement properties of the edge transport barrier (ETB) in H-mode plasmas are lost by the periodic occurrence of type I edge localized modes (ELMs). It is found experimentally that the impurity transport in-between ELMs comes down to neoclassical values. Especially, the drift parameter v/D increases with the charge of the impurity ions (He^{2+}, C^{6+}, Ne^{10+}, Ar^{16+}), in agreement with neoclassical transport predictions. The electron heat diffusivity in the ETB is anomalously high and is correlated with scale lengths down to the collisionless skin depth. Profiles of the radial electric field E_r in-between ELMs are inferred by analyzing the He II line radiation at the plasma edge. The first results are according to neoclassical expectations. With dedicated edge diagnostics the time evolutions of electron density, temperature, and pressure profiles in the ETB can now be observed during a type I ELM cycle. During the ELM crash the electron density and temperature profiles flatten. The recovery of the profiles shows some correlation: The re-steepening of the electron temperature profile stagnates when the electron density profile steepens. After the electron density and temperature profiles have gained their pre-ELM shape, no ELM appears then, but large scale fluctuations of the electron density and temperature are observed. It cannot be confirmed that the delay in the recovery of the edge current density due to current diffusion sets the time for the next ELM.

1 Introduction

H-mode plasmas [1] are characterized by particle and temperature profiles, which have a pedestal at the plasma edge. The generation of the pedestal is due to an edge transport barrier (ETB), where turbulence and the transport associated with it, is reduced. The paradigm is, that sheared $\vec{E} \times \vec{B}$ flows at the plasma edge suppress the turbulence there. The ETB is destroyed by the periodic occurrence of edge localized modes (ELMs). In discharges with type-I ELMs [2], which are investigated in this paper, ELMs typically last for about 200 μs and appear repetitively about every tens of ms. With the edge diagnostics available at ASDEX Upgrade, which have sufficiently high temporal and spatial resolution (section 2), an ELM-resolved investigation of the properties of the ETB is possible [3]. Especially the transport of impurity ions in-between the ELMs (section 3.1), and first results of radial electric field profiles determined from passive He II line radiation (section 3.2) are discussed. Additionally the recovery of the electron density and temperature profiles after the ELM crash are investigated in detail (section 3.3). When the electron pressure profile has reached its pre-ELM shape no ELM appears, but large scale fluctuations are observed. Simulations of the edge current density, however, show that the current diffusion is not the main candidate for delaying the time for the occurrence of the next ELM.

2 Diagnostics

On ASDEX Upgrade a dedicated set of diagnostics with high spatial and temporal resolution as well as high precision exists to study particle and heat transport in the ETB: The electron temperature is determined by measuring the electron cyclotron emission (ECE) of the plasma (radial resolution about 10 mm, sampling rate of the data acquisition system 31 kHz) and by Thomson scattering (TS) [4, 5] (radial resolution 3 mm, repetition rate 120 Hz). The electron density is obtained by analyzing the emission profiles of a lithium diagnostic beam (radial resolution 5 mm, temporal resolution 50 μs) [6], by Thomson scattering and by DCN laser interferometry. The data from the lithium beam diagnostic and from interferometry are used to estimate a global electron density profile in the frame work of integrated data analysis [7]. Impurity ion temperatures and densities are measured with an edge charge exchange recombination spectroscopy (CXRS) system (radial resolution 5 mm, temporal resolution 1.9 ms) [8]. With radial sweeps of the plasma and the strong radial gradient of the emission intensity finally a radial resolution of 3 mm is obtained.

The position of the magnetic separatrix has an accuracy of ± 5 mm. This is not accurate enough for pedestal studies. According to a parallel heat transport model [9] the electron temperature at the separatrix is 80-120 eV. This defines the spatial position of the separatrix in the electron temperature profiles measured by TS. The electron temperature profiles measured by ECE are aligned to the profiles measured by TS in the upper half of the pedestal, where ECE emission is optically thick. Since electron density and temperature are measured in the same scattering volume by TS, the electron density profiles measured by the lithium beam diagnostic are aligned to the profiles measured by TS.

3 Results

In the following the transport of the impurity ions, the profiles of the radial electric field in the ETB, and the re-steepening of the electron density and temperature profiles after the ELM crash, are discussed.

3.1 Transport of Impurity Ions

The discharge parameters used for the following impurity transport studies were always the same (plasma current $I_p = 1\ MA$, toroidal magnetic field $B_t = -2.5\ T$, edge safety factor $q_{95} = 4.5$, neutral beam heating power $P_{NBI} = 2.5\ MW$). The ELM frequency is around 60 Hz.

The high intensity of the C^{6+} spectral line allows to model the time evolution of the C^{6+} density profiles during the ELM cycle

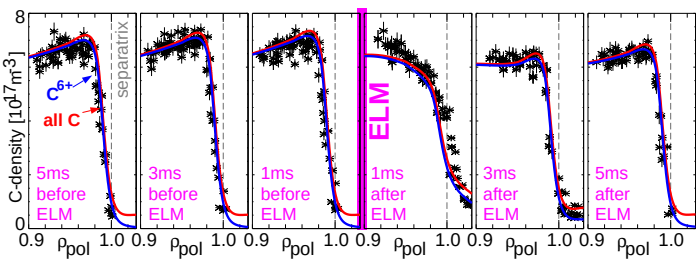

FIG. 1: ELM synchronized time sequence of C^{6+} density.

[10]. The model assumes a constant influx of neutral C. The several ionization stages are then obtained by simulating the ionization and recombination processes in the plasma with the impurity transport code STRAHL (for details see [10]). The transport is modeled by radial profiles of a diffusion coefficient D and a drift v. The effect of an ELM is taken into account by increasing the diffusion to $D = 10\ m^2/s$ for 200 μs. Inside the ETB the transport is again large due to turbulence ($D = 1\ m^2/s$). An outward pinch of $v = 1\ m/s$ is assumed here. The results of the best fit for D and v are shown in FIG. 1. The obtained agreement between measured and modeled C^{6+} density profiles is quite good for all phases during the ELM cycle, except for the time 1 ms after the ELM where deviations exist. These are most probably due to details of the time evolution of the ELM (filaments), which are not taken into account in the model. The steep gradients of the C^{6+} density between the ELMs are only possible by including an inward drift. These simulated profiles of the C^{6+} density were obtained with radial profiles of D and v shown in FIG. 2. In the center of the ETB at the magnetic coordinate $\rho_{pol} = 0.99$ the transport coefficients, including their uncertainties are $0.1 - 0.6\ m^2/s$ for D and $7 - 40\ m/s$ for v, which is in agreement with expectations from neoclassics. The neoclassical values D_{neo}, v_{neo} in FIG. 2 were taken from the code NEOART (for details see [10]).

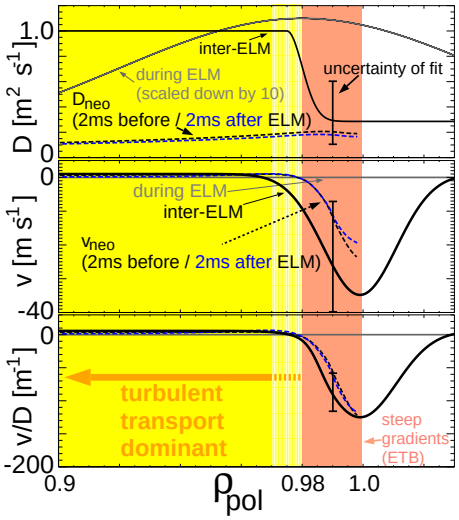

FIG. 2: Transport coefficients for C^{6+} ions.

To investigate the dependence of v and D on the charge number Z, the density profiles of intrinsic He^{2+}, C^{6+} and puffed Ne^{10+} and Ar^{16+} were measured. The profiles of Ne^{10+} and Ar^{16+} show larger scatter, so that the evolution in time during the ELM cycle, as was done for C^{6+}, is not possible. It was found, that the C^{6+} density profiles do not considerably vary with time, if taken long enough after an ELM. So for comparison of the different ions the data points from 5 ms after an ELM to 2 ms before the next ELM are accumulated in a phase ($\approx$ 600 ms) of the discharge where the impurity pedestal density

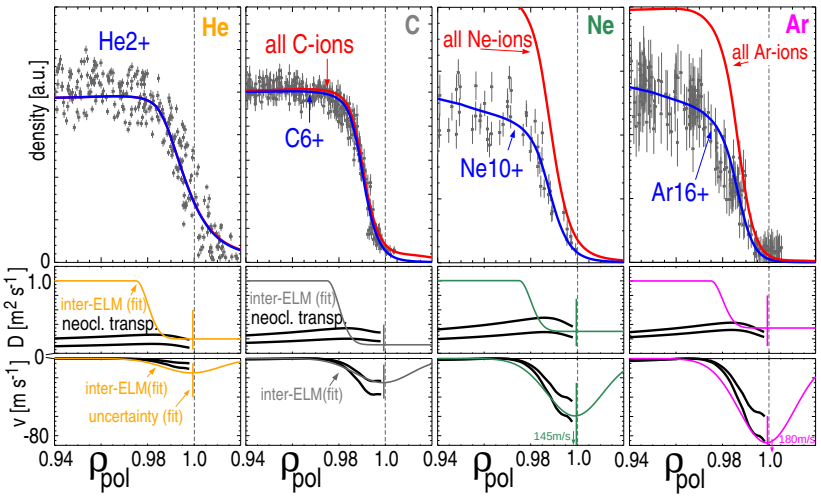

FIG. 3: Impurity densities as measured in-between ELMs.

stays constant, see FIG. 3. The obtained profiles for the transport coefficients D and v, are compared to the neoclassical predictions (just before, and just after an ELM) in FIG. 3, bottom. Within the error bars of the determined transport coefficients agreement is found to the neoclassical predictions in the ETB. Especially the necessary inward pinch increases with the charge number Z, as expected from neoclassics.

The ratios v/D at $\rho_{pol} = 0.99$ and the pedestal peaking factors $F_I = n_I(\rho_{pol} = 0.97)/n_I(\rho_{pol} = 1.0)$, with n_I as the impurity density, are shown in FIG. 4. They agree within their error bars with the neoclassical predictions.

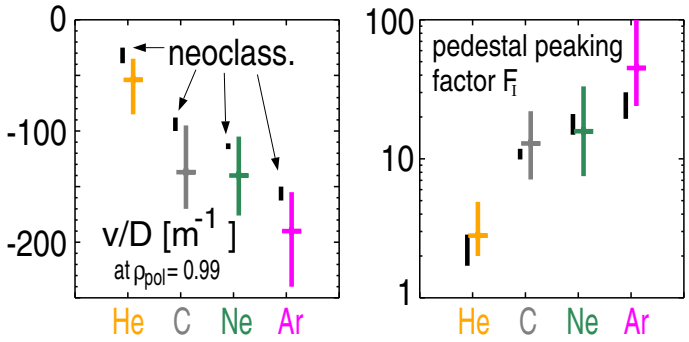

FIG. 4: Obtained drift parameters v/D and pedestal peaking factors F_I as compared to the neoclassical expectations (black).

When the pedestal of electron density and temperatures and ion temperature are known, the impurity transport can be predicted. What determines the shape of the background profiles, is still not explained.

The electron heat diffusivity in H-mode plasmas was found to be anomalously high. It scales with a very small scale, the collisionless skin-depth [11]. This may indicate that fluctuations on this scale exist at the plasma edge.

3.2 Radial Electric Field Profiles

Radial profiles of the radial electric field E_r are determined with a spectroscopic method [12]: The diagnostic consists of 18 lines of sight, which are oriented almost completely in the poloidal direction at the plasma edge, collecting the light of passive He II emission. A forward model is used to determine radial profiles of the radial electric field E_r, the temperature T_{He^+}, and density n_{He^+} of He^+ ions from the line-integrated measurements within the frame work of integrated data analysis. All three parameters determine the observed shape of the line radiation: The intensity of the line emission is proportional to the He^+ density n_{He^+}. The width of the emitted line is due to Doppler broadening, because of the thermal motion of the He^+ ions with temperature T_{He^+}. The central wavelength is Doppler shifted, because of the projection of the toroidal velocity to the line of sight, the diamagnetic velocity and the $\vec{E} \times \vec{B}$ velocity, which is dominating over the other contributions.

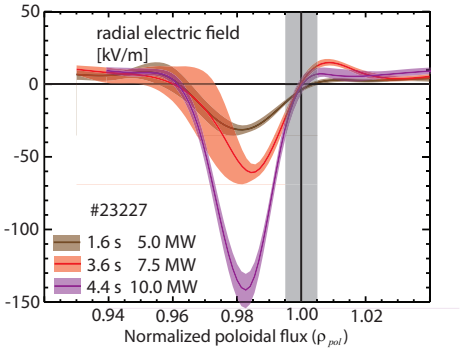

FIG. 5: Scan of the heating power.

The obtained radial and temporal resolutions are below 7 mm, and 4 ms respectively. For discharges where the distance in time between the ELMs is larger than 4 ms, ELM synchronized evaluations of the radial electric field can be done. Especially the phase in-between ELMs can be investigated and dependencies on plasma parameters can be studied.

When increasing the NBI heating power the radial electric field E_r in the ETB becomes more negative (FIG. 5). Note that uncertainties exist in the spatial position of the equilibrium (grey zone in FIG. 5), and the spatial position of the radial profiles, which are mapped from poloidally and toroidally different positions onto magnetic coordinates. Within these spatial uncertainties the E_r profiles are shifted outwards, so that the zero crossings are localized at the separatrix, or the area, where the radial electric field is positive again, is localized in the scrape-off layer. This is also observed in the radial electric field profiles measured by Doppler reflectometry on ASDEX Upgrade [13].

Increasing the deuterium fueling rate, the negative amplitude of the radial electric field E_r is reduced (FIG. 6). The width and the amplitude of the radial electric field E_r scales in the ETB with the width and amplitude of $\nabla p/n$ (p, n: pressure, density of main (deuterium) ions respectively) as expected from neoclassical theory (FIG. 7). Note that in FIG. 7 the radial positions of the $\nabla p/n$ profiles are not shifted.

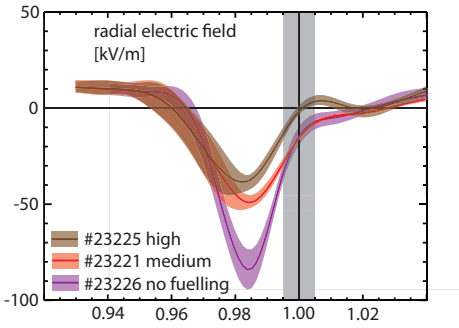

FIG. 6: Scan of D_2 fueling rate.

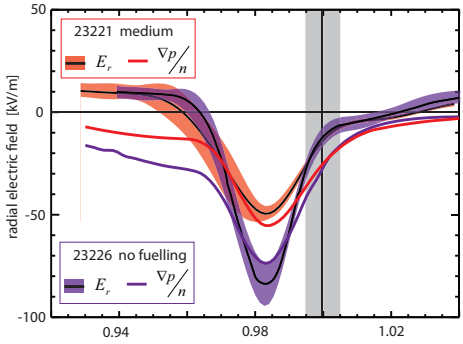

FIG. 7: E_r follows $\nabla p/n$.

3.3 Recovery of Electron Density and Temperature Profiles after an ELM

The evolution of the electron density and temperature profiles during an ELM cycle is investigated with ECE, lithium beam, and interferometric measurements, which have sufficiently high resolution in time. Of interest here is the recovery phase after the ELM crash, which is characterized by determining the maximal radial gradients of the electron temperature, ∇T_e, and density, ∇n_e. Different phases during the re-steepening of the profiles are found [14]. In FIG. 8 the profile data for 105 ELMs are plotted synchronized to the start of each ELM. Five phases can be discerned in the recovery of the T_e profiles in FIG. 8: (i) There is nearly no pedestal for around 1.5 ms, FIG. 8(c). (ii) A small pedestal develops in the next 1 ms, FIG. 8(d). (iii) Between 2.5 ms and 4 ms after the ELM crash ∇T_e stays constant. (iv) The T_e gradient enters a fast recovery phase, where it increases by more than half over 2.5 ms, FIG. 8(e). (v) The gradient of T_e increases further, but slowly, and shows a lot of scatter, FIG. 8(f). The gradient of n_e also recovers in different phases: After the loss of the pedestal after the ELM crash, FIG. 8(g), it recovers within the next 3 ms, FIG. 8(h). At around 3.5 ms after the ELM the data suggest a peaking of the n_e gradient, FIG. 8(b) and (i). This phase ends when the T_e gradient enters phase (iv). The pedestal of n_e is fully developed at later times, and shows a smooth profile,

FIG. 8(j). The apparent fluctuations of the gradient of n_e are here due to slight shifts of the pedestal top, or bottom in the steep ETB. With higher resolution Thomson scattering measurements, correlated fluctuations of n_e and T_e were found in this phase [11, 15].

In four discharges with the same plasma parameters, $I_p = 1\ MA$, $B_t = -2.5\ T$, 7.5 MW neutral beam and 1.3 MW electron cyclotron heating power, the fueling rate was varied: from no fueling for discharge #23226, to $4.0 \times 10^{21} s^{-1}$ for #23219, $5.8 \times 10^{21} s^{-1}$ for #23221, to $9.0 \times 10^{21} s^{-1}$ for #23225. A slight variation of the recovery phase is observed with the fueling rate [14]: (i) The time interval of small n_e and T_e gradients increases from 1 ms to 2 ms with increasing fueling rate (see FIG. 9). (ii) The phase of roughly constant T_e gradient, where the n_e gradient steepens gets slightly shorter with increasing fueling rate (see vertical dotted lines in FIG. 9).

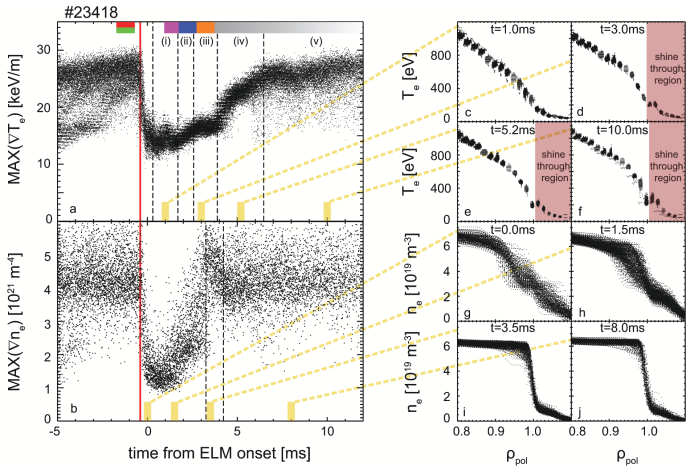

FIG. 8: ELM-synchronized maximal ∇T_e (a) and ∇n_e (b), T_e profiles (c-f) and n_e profiles (g-h) for the indicated times relative to the ELM.

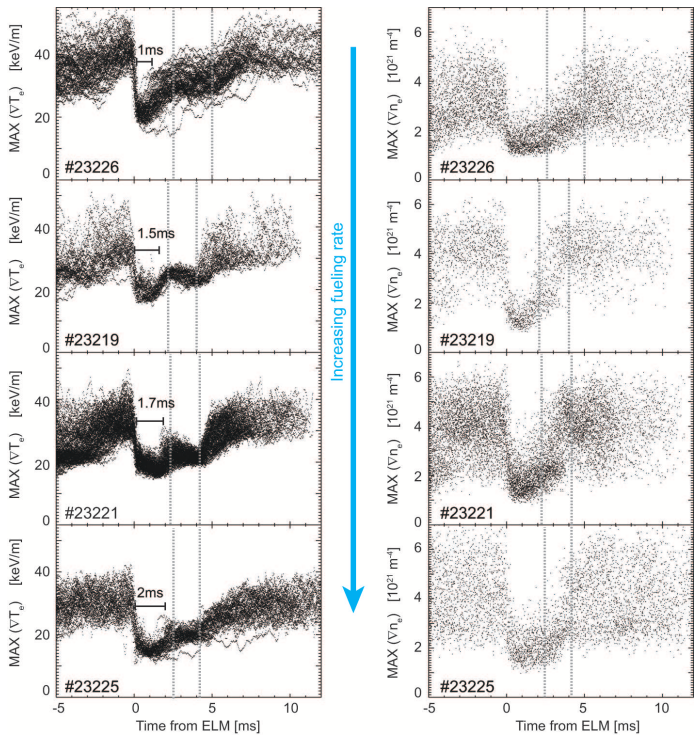

FIG. 9: ELM-synchronized maximal ∇T_e and ∇n_e for several fueling rates.

According to the peeling-ballooning model the occurrence of an ELM is set by a sufficiently large edge current density, which drives the peeling mode instability. The recovery of the edge current was therefore modeled with a current diffusion equation. The total current does not change on the time scales of interest, because the inductivity of the plasma is so large. Only the bootstrap current, which is driven by the electron density and temperature gradients and the ion temperature gradients, and which is delayed by current diffusion, can play a role (for details see [14]).

Since the profiles have become flat (FIG. 10(a), (b)) during the ELM crash, the bootstrap current also collapses (FIG. 10(c), red). The total current density changes much more

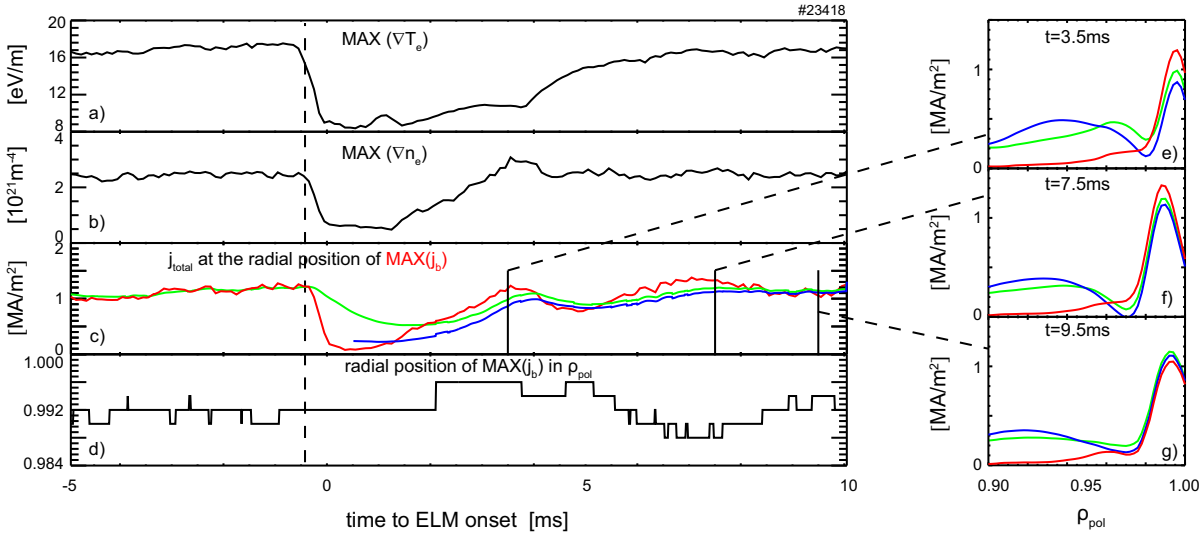

FIG. 10: Time traces of maximal ∇T_e (a) and ∇n_e (b) and the maximal bootstrap current (red) and the maximal total current density for two different starting times (green, blue) (c) at the position ρ_{pol} (d), as well as radial profiles of the current densities at different times in the ELM cycle (e-g).

slowly due to current diffusion (FIG. 10(c), green). The recovery of the total current density follows the bootstrap current with a delay of only about 1 ms, which is not enough to explain the long delay to the next ELM. Even when assuming that during the ELM crash the total edge current density is lost by current carrying filaments, the total current density (FIG. 10(c), blue) recovers nearly as fast as ∇n_e and ∇T_e, and the delay until the occurrence of the next ELM is not yet explained.

4 Summary and Conclusions

On ASDEX Upgrade a dedicated set of diagnostics with sufficiently high temporal and spatial resolution exists, to characterize the transport of ions and electrons in the ETB.

It is found experimentally that for the impurity ions He^{2+}, C^{6+}, Ne^{10+}, Ar^{16+} the transport in the ETB comes down to values expected from neoclassics. This includes the observation that the drift parameter v/D increases with the charge of the impurity ions. The determination of the transport coefficients at the pedestal with various impurity ions at the same plasma conditions has been done for the first time. The obtained transport results are used as input for a transport model for tungsten, which cannot be investigated directly [10]. The transport of the electrons remains anomalous in the ETB.

The radial electric field profiles, determined from passive He II emission in-between ELMs, scale with $\nabla p/n$ of the main ions (deuterium) according to neoclassical expectations. The amplitude of the radial electric field increases with NBI heating power and decreasing fueling rate.

The evolution of the electron density and temperature profiles after an ELM are followed with the ECE and lithium beam diagnostics. The electron density and temperature profiles recover in several stages, which are correlated: The electron density profile has recovered to its pre-ELM shape after 3.5 ms after the ELM. The re-steepening of the

electron temperature profile has several phases: Especially when the electron density profile steepens with the fastest rate during the ELM cycle, no increase of the electron temperature gradient is observed. After the electron pressure profile has reached its pre-ELM shape in general no ELM appears, but large scale fluctuations are observed. It could not be confirmed that a delay in the build-up of the edge current density due to current diffusion plays a significant role in setting the time for the next ELM.

References

[1] WAGNER, F., et al., "Regime of Improved Confinement and High Beta in Neutral-Beam-Heated Divertor Discharges of the ASDEX Tokamak", Phys. Rev. Lett. **49** (1982) 1408

[2] SUTTROP, W., "The physics of large and small edge localized modes", Plasma Phys. Control. Fusion **42** (2000) A1

[3] WOLFRUM, E., et al., "Investigation of inter-ELM pedestal profiles in ASDEX Upgrade", Plasma Phys. Control. Fusion **51** (2009) 124057

[4] MURMANN, H.-D., et al., "The Thomson scattering systems of the ASDEX upgrade tokamak", Rev. Sci. Instrum. **63** (1992) 4941

[5] KURZAN, B., et al., "Signal processing of Thomson scattering data in a noisy environment in ASDEX Upgrade", Plasma Phys. Control. Fusion **46** (2004) 299

[6] FISCHER, R., et al.,"Probabilistic lithium beam data analysis", Plasma Phys. Control. Fusion **50** (2008) 085009

[7] FISCHER, R., et al., "Integrated data analysis of profile diagnostics at ASDEX Upgrade", Fusion Sci. Techn. **58** (2010) 675

[8] PÜTTERICH, T., et al., "Evidence for Strong Shear of Toroidal Rotation at the Edge-Transport Barrier in the ASDEX Upgrade", Phys. Rev. Lett. **102** (2009) 025001

[9] NEUHAUSER, J., et al., "Transport into and across the scrape-off layer in the ASDEX Upgrade divertor tokamak", Plasma Phys. Control. Fusion **44** (2002) 855

[10] PÜTTERICH, T., et al., "ELM flushing and Impurity Transport in the H-mode Edge Barrier in ASDEX Upgrade", 19th International Conference on Plasma Surface Interactions, San Diego (2010) I-14

[11] KURZAN, B., et al., "Scale lengths of inter-ELM fluctuations in the pedestal of ASDEX Upgrade", Plasma Phys. Control. Fusion **51** (2009) 065009

[12] WIELAND, B., et al., "Radial electric fields from passive He II emission in the edge transport barrier of ASDEX Upgrade", 37th EPS conference, Dublin (2010) P5.139

[13] CONWAY, G., et al., "Plasma rotation profile measurements using Doppler reflectometry", Plasma Phys. Control. Fusion **46** (2004) 951

[14] BURCKHART, A., et al., "Inter-ELM behaviour of the electron density and temperature pedestal in ASDEX Upgrade", Plasma Phys. Control. Fusion **52** (2010) 105010

[15] KURZAN, B., et al., "Thomson scattering analysis of large scale fluctuations in the ASDEX Upgrade edge", Plasma Phys. Control. Fusion **49** (2007) 825